Author Manuscript

Author Manuscript

Author Manuscript

Author Manuscript

HHS Public Access

Author manuscript

Adv Healthc Mater. Author manuscript; available in PMC 2024 November 01.

Published in final edited form as:

Adv Healthc Mater. 2023 November ; 12(28): e2301280. doi:10.1002/adhm.202301280.

A miniaturized, battery-free, wireless wound monitor that predicts wound closure rate early

Nate T. Garland[1,2,†], **Joseph W. Song**[3,4,5,†], **Tengfei Ma**[6,†], **Yong Jae Kim**[1,2,†], **Abraham Vázquez-Guardado**[4,‡], **Ayemeh Bagheri Hashkavayi**[1,2], **Sankalp Koduvayur Ganeshan**[2,§], **Nivesh Sharma**[1,2], **Hanjun Ryu**[4,‖], **Min-Kyu Lee**[4], **Brandon Sumpio**[7], **Margaret A. Jakus**[8], **Viviane Forsberg**[4,9], **Rajaram Kaveti**[1,2], **Samuel K. Sia**[8], **Aristidis Veves**[7], **John A. Rogers**[3,4,5,10,11,12,*], **Guillermo A. Ameer**[3,4,5,13,14,15,16,*], **Amay J. Bandodkar**[1,2,17,*]

[1]Department of Electrical and Computer Engineering, North Carolina State University, Raleigh, NC, USA.

[2]Center for Advanced Self-Powered Systems of Integrated Sensors and Technologies (ASSIST), North Carolina State University, Raleigh, NC, USA.

[3]Department of Biomedical Engineering, Northwestern University, Evanston, IL, USA.

[4]Querrey Simpson Institute for Bioelectronics, Northwestern University, Evanston, IL, USA.

[5]Center for Advanced Regenerative Engineering, Northwestern University, Evanston, IL, USA.

[6]IBM T. J. Watson Research Center, Ossining, NY, USA.

[7]Joslin-Beth Israel Deaconess Foot Center and the Rongxiang Xu, MD, Center for Regenerative Therapeutics, Beth Israel Deaconess Medical Center, Harvard Medical School, Boston, MA, USA.

[8]Department of Biomedical Engineering, Columbia University, USA.

[9]Department of Natural Sciences, Mid Sweden University, Holmgatan 10, 851 70, Sundsvall, Sweden.

[10]Department of Materials Science and Engineering, Northwestern University, Evanston, IL, USA.

[11]Department of Mechanical Engineering, Northwestern University, Evanston, IL, USA.

[12]Department of Neurological Surgery, Feinberg School of Medicine, Northwestern University, Evanston, IL, USA.

[13]Simpson Querrey Institute for Bionanotechnology, Evanston, IL, USA.

[14]Chemistry of Life Processes Institute, Northwestern University, Evanston, IL, USA.

[*]Corresponding authors: John A. Rogers (jrogers@northwestern.edu); Guillermo A. Ameer (g-ameer@northwestern.edu); Amay J. Bandodkar (ajbandod@ncsu.edu).
[†]These authors contributed equally to this work.
[‡]Present address: Department of Electrical and Computer Engineering, North Carolina State University, Raleigh, NC, USA.
[§]Department of Materials Science and Engineering, Northwestern University, Evanston, IL, USA.
[‖]Department of Advanced Materials Engineering, Chung-Ang University, Anseong, Korea.

Supporting Information

Supporting Information is available from the Wiley Online Library or from the author.

Conflict of Interest: The authors declare that they have no other competing interests.

Author Manuscript Author Manuscript Author Manuscript Author Manuscript

[15]Department of Surgery, Feinberg School of Medicine, Northwestern University, Chicago, IL, USA.

[16]International Institute for Nanotechnology, Northwestern University, Evanston, IL, USA

[17]Joint Department of Biomedical Engineering, North Carolina State University and University of North Carolina at Chapel Hill, NC, USA.

Abstract

Diabetic foot ulcers are chronic wounds that affect millions, and increase the risk of amputation and mortality, highlighting the critical need for their early detection. Recent demonstrations of wearable sensors enable real-time wound assessment, but they rely on bulky electronics, making them difficult to interface with wounds. Here, we introduce a miniaturized, wireless, battery-free wound monitor that measures lactate in real-time and seamlessly integrates with bandages for conformal attachment to the wound bed. We select lactate due to its multifaceted role in initiating healing. Studies in healthy and diabetic mice reveal distinct lactate profiles for normal and impaired healing wounds. A mathematical model based on the sensor data predicts wound closure rate within the first three days post-injury with ~76% accuracy which increases to ~83% when pH is included. These studies underscore the significance of monitoring biomarkers during the inflammation phase, which can offer several benefits, including short-term use of wound monitors and their easy removal, resulting in lower risks of injury and infection at the wound site. Improvements in prediction accuracy can be achieved by designing mathematical models that build on multiple wound parameters such as pro-inflammatory and metabolic markers. Achieving this goal will require designing multi-analyte wound monitors.

Graphical Abstract

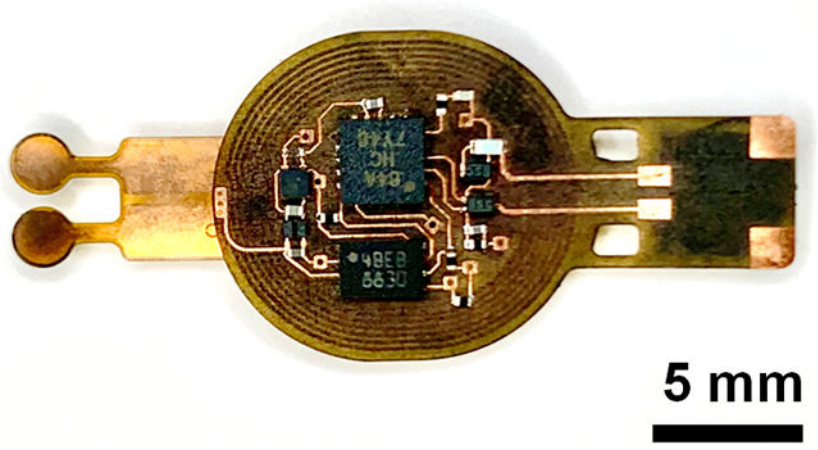

A biofuel cell-based lactate sensor coupled with wireless, battery-free electronics for real-time wound monitoring and prediction of wound closure rate.

Keywords

Diabetic ulcers; chronic wounds; wound sensing; wireless electronics; lactate sensing

Author Manuscript Author Manuscript Author Manuscript Author Manuscript

1. Introduction

Diabetic foot ulcers (DFUs) affect approximately 750,000 individuals and are responsible for around 70,000 amputations per year in the US alone.[1] Chronic wounds, including DFUs, carry a 5-year mortality rate of 30.5%, which is comparable to cancer's mortality rate of 31%.[2] The economic burden of treating chronic wounds is staggering, as it accounts for approximately 1-3% of total healthcare expenditure in most developed countries.[3] The ongoing diabetes epidemic and ever-increasing healthcare costs are expected to worsen the grim statistics for DFUs in the foreseeable future.[4] Studies indicate that providing wound-specific care in a timely manner can significantly reduce treatment costs, amputation risk, and mortality.[3]

Assessment tools that accurately capture wound status in real-time are key for prescribing tailored treatments. Unfortunately, present methods rely on intermittent removal of the dressing followed by visual analysis or wound culture test.[5,6] The former lacks necessary diagnostic and prognostic rigor, while the latter is time-consuming and requires sophisticated instruments and trained personnel. Moreover, these methods do not provide real-time status of the wounds. Smart bandages that incorporate sensors for longitudinal monitoring of metabolites, pH, temperature, oxygen, and bacteria in wound exudate offer unique potential for accurate, at-home wound assessment.[7-19] Such advanced sensors can provide previously unavailable real-time insights into wound physiology. While such wearable embodiments are a major advancement in the field of wound care, they usually rely on bulky, complex wireless electronics that preclude their use in constricted body parts (foot, sacrum) most prone to chronic wounds. Furthermore, much of the work in this field focuses on demonstrating the viability of sensors for monitoring wound composition, with little emphasis on interpreting these results for predicting the future course of healing, such as wound closure rate. Demonstrating such capabilities will enable clinicians to recommend wound-specific treatments for rapid closure.

This article describes a miniaturized wound monitor that longitudinally assesses wounds and predicts wound closure with ~76% accuracy within the first 3 days post-injury in a rodent model of DFU (Figure 1A). It weighs ~160 mg with dimensions of 28 mm x 12 mm x 0.2 mm. The monitor achieves its miniaturized formfactor and low weight without compromising on performance by combining disparate technologies involving biofuel cells and battery-free wireless electronics. The robust, thin, miniaturized device reduces risks of injury and is amenable for applications in constricted body regions, for example devices applied to the heel – a region at high risk of developing chronic wounds.

The device detects wound lactate levels using a self-powered biofuel cell-based sensor and transmits the data wirelessly using nearfield communication (NFC) protocols. A mathematical model interprets the sensor data to identify the nature of the wound (normal or diabetic) and predict wound closure rate. Figure 1B shows an exploded view illustration of the wound monitor. Figure 1C shows an image of the wireless electronics while Figure 1D shows a photo of the complete wound monitor. Lactate is selected as the biomarker of interest due to its multi-faceted role in wound healing.[20-23] Studies show that wound lactate in the ~5-15 mM range is necessary to initiate various aspects

Author Manuscript Author Manuscript Author Manuscript Author Manuscript

of wound healing such as hypoxia-inducible factor-1α stabilization;[20] growth factor and metalloproteinases production;[22,24] endothelial cell mobility,[25] vascularization;[20] increased collagen synthesis,[22,26] among other processes.[27,28] However, abnormal lactate levels hinder wound healing: high levels delay healing due to severe hypoxia, while low levels impede initiation of the healing process.[20] The present work exploits these unique prognostic properties of wound lactate for demonstrating the miniaturized wound monitor's capacity to predict wound closure rate early. This marks a major advancement in the field of wound care as information provided by the described wound monitor will be useful for timely course correction if the present treatment is not expected to lead to rapid wound closure. Table S1 (Supporting Information) compares present work with some recent representative examples of wound monitors.

2. Results

2.1 UV sterilizable, self-powered, oxygen-independent, biofuel cell-based lactate sensor

Electrochemical enzymatic sensors, such as lactate sensors, typically rely on amperometry to detect analytes.[29] However, this technique requires bulky potentiostats and batteries for data acquisition as illustrated by recent examples of wearable sensors, including some for wound assessment analytes.[30-37] These sensors typically use Bluetooth connectivity for wireless data transmission, further increasing device size and energy requirements. Our work on self-powered, NFC-enabled, biofuel cell-based sensors offers a lighter and smaller alternative to battery-powered sensors without compromising on performance,[38] thus representing an attractive technology for realizing wound monitors. The sensor works by lactate spontaneously oxidizing at the anode and silver oxide reducing at the cathode, producing a lactate concentration-dependent current signal. Figure S1A (Supporting Information) shows the spontaneous, catalytic reactions occurring at the sensor anode and cathode that result in the current signal. Similar biofuel cell-based sensing principles for lactate detection are reported by several groups.[39-42] A resistor (100 kΩ) converts this current signal to a voltage signal, which is wirelessly transmitted to a nearby reader (e.g. laptop or smartphone) using NFC electronics.

Figure 2A shows schematic representation of the key components of the sensor. Laser patterned gold on polyimide films form the bare anode and cathode electrodes of the sensor. A film of 3D carbon nanotube (CNT) paper bonded onto the active area of the anode enhances electrochemical active surface area and its absorptive properties minimize leaching of the reagents. Immobilizing tetrathiafulvalene and lactate oxidase on the CNT paper enables selective, low overpotential oxidation of the lactate at the anode. Unlike typical cathodes in biofuel cells that rely on oxygen reduction reactions,[43-49] the cathode of the lactate sensor depends on oxygen-independent reduction reaction of immobilized silver oxide[50-52] which ensures fluctuations in wound oxygen levels do not affect sensor response.[53-56] The complete sensor is coated with chitosan and polyvinyl chloride membranes to extend detection range and reduce leaching of reagents.

UV treatment is a widely used sterilization technique for medical devices including wound care products.[57,58] Unfortunately, UV exposure denatures enzymes (here lactate oxidase) which results in a decrease in sensor sensitivity. Covering the sensor with widely used

Author Manuscript Author Manuscript Author Manuscript Author Manuscript

UV protective films or absorbers could resolve this issue.[59-61] However, the poor mass transport across the former and the potential toxicity of the latter are limitations. The lactate sensor incorporates an unconventional UV protective membrane that overcomes these limitations. It involves edible carbon suspended in chitosan matrix. The edible carbon blocks the UV light while the porous nature of the edible carbon/chitosan composite facilitates rapid transport of the analyte to the sensor surface. Moreover, this membrane serves as a biocompatible interface between the sensor and the wound, allowing a normal course of healing while minimizing foreign body response. Figure 2B shows an image of the lactate sensor.

2.2 In vitro characterization of the lactate sensor

Figure 2C shows the lactate sensor's typical response when exposed to repeated cycles of lactate, while Figure 2D shows the sensor's stabilized signals for the reversibility test. The near-overlapping signals demonstrate the sensor’s negligible hysteresis necessary for longitudinal wound assessment. Figure 2E shows that increasing the thickness of the polyvinyl chloride diffusion membrane extends the linear detection range from ~15 mM to ~30 mM. Figure 2F shows the corresponding calibration plot. The limit of detection (LOD) for the lactate sensor is 0.47 mM. LOD is calculated as $3 \times S_b/S$, where S_b is the standard error of the baseline response and S is the slope of the calibration curve.[38] Such modification improves the linear detection range, but results in slower response time (~5 min). Each sensor undergoes calibration before use to accommodate for variability in baseline signal. This is a common strategy employed by many commercial chemical sensors and is useful in ensuring reliable sensor data interpretation. Figure 2G demonstrates negligible interference on the sensor response due to presence of glucose (3 mM), uric acid (100 μM), creatinine (200 μM), and ascorbic acid (500 μM). The concentrations of these chemicals are based on their physiological concentrations in wound exudate.[62] Figure 2H exhibits the effect of UV sterilization. Standard UV sterilization parameters (power: 40 μW/cm^2; wavelength: 254 nm; duration: 30 min) are used for these studies. A decrease in sensor sensitivity of around 65% is noted for sensors without the UV protective coating, while this percentage for sensors with the coating is only ~6% after UV sterilization. The negligible decrease in sensitivity for the sensors with the UV protective coating can be attributed to the near-complete blocking of the 254 nm UV light (transmittance ~7%) used for sterilization and facile transport of the lactate through the porous UV protective membrane (Figure S1B and S1C, Supporting Information). We did not study the effectiveness of the UV protective film for extended periods of UV treatment (> 30 min). Systematic investigation of UV protective film thickness and treatment parameters will be a subject of future research.

Figure 2I reports data investigating the long-term sensor stability over a period of 10 days under conditions mimicking a typical wound. The experiment involves storing the sensors in ambient conditions interfaced with a phantom wound (agarose membrane) and recording daily sensor response. The data reveals that the sensors maintain their response up to day 7, with a slight increase in sensor sensitivity observed up to day 3. This can be attributed to swelling of the chitosan and polyvinyl chloride membranes resulting in increased diffusion of lactate towards the sensor. Noticeable signal degradation is observed beyond day 7. The ability of the sensor to reliably monitor lactate in the initial 7-day period

Author Manuscript Author Manuscript Author Manuscript Author Manuscript

is sufficient for its capacity for predicting wound closure as described later. Additional studies reported in Figure 2J evaluate the biofouling of sensors when continuously exposed to artificial wound exudate prepared per literature.[63] The data reveals a ~20% decrease in sensor sensitivity after exposure to the artificial wound exudate which probably arises from adsorption of proteins present in it onto the sensor surface. The in vivo studies (described later) take this signal decrement into account while estimating lactate concentration. Figure S1D (Supporting Information) exhibits the effect of pH on sensor response. The data shows that the sensitivity is negligibly affected in the physiologically relevant range of pH 3-8. The minimum volume of wound fluid necessary for reliable sensor data is estimated by placing phantom wounds with varying amounts of fluid and recording sensor data. The phantom wound is comprised of cellulose membrane (Kimwipe™) soaked with known volume of buffer. Figure S1E (Supporting Information) shows that only ~80 nL/mm^2 fluid is sufficient for the sensor to acquire ~95% of the saturation signal which makes the sensor suitable for monitoring wounds with low volumes of wound fluid. Advanced version of the wound monitor could include a separate impedance sensor for recording wound fluid level which could be used to compensate for variations in lactate sensor signal due to changes in fluid amount.

2.3 Biocompatibility tests of the lactate sensor

Figure 3A shows live/dead staining of L929 mouse fibroblasts cultured separately over the anode and cathode for 96 h, along with the positive control (no electrode). The data reveals that the sensor has no significant influence on cell survival when compared to the control. Results of cell viability assay also show no signs of sensor cytotoxicity (Figure 3B).

Testing the effect of sensor on wound closure rate involves applying a sensor to a splinted, full-thickness excisional dermal wound in healthy and diabetic mice and evaluating the changes in wound area over a period of 10 days. The splinted, full-thickness excisional dermal wound is selected as it minimizes wound healing due to skin contraction and enables a healing process similar to that in humans.[64-66] Figure 3C represents the healing progression of four groups: healthy mice with/without a sensor and diabetic mice with/without a sensor. All groups receive no treatment other than a protective dressing (Tegaderm™). Digital pictures of the wounds captured on day 1, 5, 7, and 10 post-injury reveal no significant difference in wound closure between the study groups, indicating the negligible impact of the sensor on the wound healing rate (Figure 3D and 3E). Specifically, for healthy mice without a sensor, 89.0 ± 3.8 % closure occurs on day 10 compared to 88.7 ± 4.6 % for the healthy mice with a sensor. For diabetic mice without a sensor, 42.5 ± 16.5 % closure occurs on day 10 compared to 43.6 ± 7.7 % for diabetic mice with a sensor. The slower healing rate in diabetic animals can be attributed to the delayed healing caused by diabetes.[67] The sensor can be easily removed without damaging the newly grown tissue at the end of the study (day 10). Figure S2 (Supporting Information) compares images of a fully healed wound in a healthy mouse (day 14) after the sensor is removed on day 10 to that in the control group (no sensor). The wound closure in both the cases is identical further illustrating that the application and the subsequent removal of the sensor has negligible interference with the natural healing process.

Author Manuscript Author Manuscript Author Manuscript Author Manuscript

The sensor also does not affect skin remodelling, as demonstrated by additional histological studies. Figure 2F shows the results of haematoxylin and eosin (H&E) staining of the wounded tissue on day 10 post-injury. There are no observable foreign body responses in healthy or diabetic mice. Furthermore, H&E staining of the fully healed tissue on day 30 post-injury demonstrates that the formation of the epithelial and connective tissue is similar in all the groups, indicating that the biocompatible sensor does not disturb the epithelial coverage, thickness, or granulation tissue formation.

2.4 Longitudinal wound monitoring in mice with wired lactate sensors

In vivo studies involve creating a full-thickness excisional dermal wound in diabetic and healthy mice followed by applying a sensor to the wound bed. Applying Tegaderm™ over the sensor firmly secures it to the wound bed. Three lactate concentration measurements are taken per day for the first 6 days, followed by a single point assessment until day 10. Data collection step entails attaching the sensor to a multimeter via detachable wired connectors. Figure 4A illustrates the setup, while Figure 4B shows a sensor applied to a wound in a diabetic mouse. Wound closure rate estimation involves image analysis of wound pictures captured on day 1, 5, 7, and 10. Figure 4C presents the longitudinal lactate and wound closure rate profiles for healthy and diabetic mice. Evaluation of these profiles reveals that the lactate concentration typically peaks during the first 3 days post-injury, and that the peak concentration for diabetic mice is higher than the normal wound lactate range (5-15 mM) observed in healthy mice (Figure 4D).[20] As expected, the wound closure rate in diabetic mice is slower than that in healthy ones. More specifically, all diabetic wounds show wound closure of less than 60% while healthy ones show greater than 80% closure by day 10. In the case of diabetic wounds, 8 mice show lactate outside the normal range of 5-15 mM (six animals show >15 mM and two animals show < 5 mM). Two diabetic wounds are outliers and show lactate in the normal range (5-15 mM). In the case of healthy mice, 9 animals show lactate in or very close to healthy range (5-15 mM) while only one is an outlier (lactate concentration > 15 mM). The outliers in each cohort could be attributed to a combination of reasons including extent of diabetes development and variability in healing process in individual animals, and potential fabrication variations in individual sensors. Data for individual animals appear in Figure S3 and S4 (Supporting Information).

Additional experiments assessing wound pH in healthy and diabetic mice investigate the physiological relevance of pH in wound monitoring. Developing pH assays involves excising commercial pH strips into 1 mm pads and affixing them onto flexible polyethylene terephthalate strips. Incorporating additional black and white color reference markers compensates for variations in ambient lighting conditions. Figure S5A (Supporting Information) shows a pH sensor while Figure S5B (Supporting Information) shows its calibration. Figure 4E shows a clear distinction between the pH levels for wounds in healthy and diabetic mice. Consistent with the literature, the wound pH in healthy animals becomes progressively more acidic, while it becomes slightly alkaline for wounds in diabetic mice over the period of assessment. These studies strongly support the prognostic properties of these wound biomarkers.

Author Manuscript Author Manuscript Author Manuscript Author Manuscript

A separate pilot study involves applying a sensor to the heel of a healthy human subject (male; weight: 70 kg). The heel is selected as the region of interest due to its high risk of developing chronic wounds.[68] The subject continuously walks for 30 min followed by standing still for 15 min. The cyclical and continuous loading on the sensor does not bear any effect on its performance (Figure S5C, Supporting Information) thus illustrating its ability to monitor soft tissue injury in constricted body parts under mechanical load.

2.5 Mathematical model for predicting wound closure rate

A mathematical model is developed to predict wound closure rates based on the input of lactate time series. The lactate time series is comprised of lactate concentrations for the first three days post-injury for each mouse. To understand the data and their groups, the lactate time series for every mouse are projected into a two-dimensional visual space using t-distributed stochastic neighbour embedding (t-SNE).[69] t-SNE is a commonly used dimension reduction algorithm which maps similar instances to nearby dots in a low-dimensional space. As shown in Figure 5A the diabetic and healthy groups are easily separated using the lactate time series, but it exhibits some outliers (circled in red). Steps to improve the accuracy of prediction involve deriving new features such as (a) utilizing Fast Fourier Transform (FFT) to transform the lactate time series into the frequency domains and using the corresponding Fourier coefficients for each frequency as the “frequency features” and (b) computing lactate concentration gradients between two consecutive days for each mouse as the “difference features”.[70]

Next, feeding these features into a support vector machine (SVM) generates a model that predicts whether the wound closure rate by day 10 will exceed 70%.[71] Wounds that exhibit a closure rate above 70% by day 10 indicate normal healing, whereas those with a closure rate below 70% are indicative of impaired healing. Using a 5-fold cross-validation is necessary for accurate model evaluation due to the limited number of samples. Each training set includes 16 randomly selected mice data and the testing set contains the remaining 4 mice data. We repeat this 5 times to generate the model and calculate the error in its prediction capabilities. This technique estimates the expected level of fit of a model to a data set that is independent of the data used to train the model. Initially, all samples are separated into five folds. The SVM model then undergoes iterative training on four of these folds and testing on the remaining fold. Figure 5B presents the mean accuracy of all test folds. The model points to the attractive prognostic properties of wound lactate with the capacity to predict wound closure with ~76% accuracy. The accuracy increases to ~83% if pH and lactate data are combined (Figure 5C). The error bars reported in Figure 5C can be attributed to the small sample size. While the 5-fold cross-validation step involved in generating the model helps reduce error and bias, the prediction model can be further refined to achieve higher accuracy by increasing the sample size. Nevertheless, the data reported in Figure 5 reveals that wound monitoring may be most relevant during the inflammation phase (day 1-3 post injury)[72] after which the monitor can be removed. A major benefit of such brief monitoring is the ability to easily remove the devices and avoid strong device-tissue adhesion that can cause tissue damage during the device removal process.[16,73]

Author Manuscript Author Manuscript Author Manuscript Author Manuscript

2.6 Wireless, battery-free monitoring of lactate in freely moving mice

Demonstration of wound monitoring in freely moving animals involves interfacing the lactate sensor to a custom-designed, wireless electronic module. The device leverages developments in battery-free, active electronics that support NFC and wireless power transfer via resonant magnetic induction.[74-76] Figure 6A shows the block diagram describing the device operation while Figure S6A (Supporting Information) depicts the detailed circuit design. An NFC system on chip (M24LR04E, STMicroelectronics) supporting the protocol ISO 15693 enables bidirectional communication between a remote personal computer and the wireless electronics. This facilitates tailoring control and configuration commands in real-time to gain functional access to the device for controlling the modalities of operation and its configuration (sampling rate and on-chip sample averaging). Figure S6B (Supporting Information) shows a screen shot of the Graphics User Interface. At the core of the device is a low power 8-bit microcontroller (μC, Attiny84, Atmel Corporation) flashed with a specialized firmware that permits data collection from the sensor and synchronizes data communication via NFC. Data collection is carried out with a 10-bit analog to digital converter (ADC, 1.07 mV/ADC resolution) to digitalize the sensor signal with high accuracy (Figure 6B) even at high inclination angles (Figure 6C) and across the entire experimental arena, for example, a mouse cage (Figure 6D). Data is stored in the NFC chip and then retrieved wirelessly. The use of a 32-byte cyclic buffer, controlled locally by the μC and remotely in the data recording application, allows for loss-less data transmission from the sensor in real-time during ambulatory animal testing. Maintaining the sensor in open circuit condition during idle time (period during which wound is not assessed) is essential to avoid undesired draining of the biofuel cell-based sensor. Incorporating two n-channel metal oxide field effect transistors (n-MOSFETs) within the circuit achieves this goal. Figure S6C (Supporting Information) shows the results.

In vivo studies entailing wireless assessment of wound lactate in a freely moving diabetic mouse over a period of four days post-injury validate the wireless wound monitor (Figure 6E and 6F). The duration and frequency of data acquisition is based on results acquired in experiments involving the wired sensors (Figure 4). Data plotted in Figure 6F shows a similar dramatic initial rise in wound lactate that peaks at levels higher than normal wound lactate concentration for the diabetic mouse as observed in the cohort assessed by the wired sensors (Figure 4C, bottom plot). These in vivo and in vitro studies reveal that the wireless sensors offer performance similar to the wired sensors in awake, freely moving animals without cumbersome tethers. Such wireless platforms will be useful for real-time assessment of wounds in humans as well as for a wide spectrum of basic wound research in freely moving animals.

3. Conclusion

The article describes a seamless combination of biofuel cell-based, self-powered sensing technology with battery-free wireless electronics and mathematical models for developing a wound monitor that predicts wound closure rates. The complete device weighs only 160 mg and measures 28 mm x 12 mm x 0.2 mm, making it attractive for easy integration with bandages and conformal attachment to wounds. Methodical in vitro and in vivo assessments

Author Manuscript Author Manuscript Author Manuscript Author Manuscript

of the wound monitor reveal its robustness and potential for real-life applications. The sensor exhibits a reversible response to lactate concentrations, negligible response to interfering chemicals, and a lifespan of around a week in simulated wound conditions. A UV protective, analyte-diffusible membrane encapsulation allows UV sterilization of the sensor without deteriorating its performance. Similarly, benchtop studies of wireless electronics demonstrate their capabilities to reliably capture and transmit sensor data. In vivo studies encompass wound lactate assessment in a splinted, full-thickness excisional dermal wound model in healthy and diabetic mice. A model trained on the lactate data reveals the prognostic properties of wound lactate in predicting wound closure rate within the first three days post-injury with ~76% accuracy. Additional training of the developed model with pH, measured using colorimetric pH sensors, improves the accuracy to ~83%. Multi-parametric wound monitors that measure additional wound parameters such as cytokines and other metabolites can help further improve the accuracy of the prediction model. The studies reveal the potential clinical relevance of wound monitoring during the initial days post-injury. A key benefit of such short-term wound assessment includes the ability to easily remove the bandage-integrated sensors without harming the newly formed fragile tissue. The prognostic capabilities of the developed wound monitor will be useful to key stakeholders, including patients, caregivers, and doctors. The device's ability to predict wound closure rates early is also useful in basic wound research as it can shine new light on wound healing mechanisms and help screen new wound care products. The device designs, sensing principles, and mathematical models described here lay the foundations for new classes of miniaturized monitors for accurate wound assessment.

4. Experimental Section

Fabrication of lactate sensor

Electron beam evaporation (AJA International Inc., MA, USA) formed a thin film of chromium (thickness, 10 nm) as an adhesion layer, followed by a layer of gold (Au; thickness, 100 nm) as a conductor on a 75-mm thick sheet of polyimide (PI; Argon Inc., CA, USA). A UV laser (ProtoLaser U4, LPKF Laser & Electronics, Germany) patterned the gold-coated polyimide sheet to define the separate anode and cathode circular active areas, interconnects, and contact pads.

Cathode fabrication began by mixing silver and silver oxide powder (Sigma-Aldrich, MO, USA) in a 3:7 (w/w) ratio in 2.5 wt% ethanolic Nafion suspension (Sigma-Aldrich, MO, USA) with total solid concentration of 1 g/ml. Applying a thin layer of carbon ink followed by immediate drop casting 2.5 μL of the above silver/silver oxide solution and baking at 100 °C adhered the active materials to the cathode active area.

Next, anode fabrication began with applying a thin layer of carbon ink (E3178 Carbon ink, Ercon, MA, USA) to the anode active area followed by attaching a CNT paper pad (diameter: 2mm; Buckypaper, GSM 20; NanoTechLabs, NC, USA) to it and baking at 100 °C prepared the anode transducer surface. Next, applying 2 μL of 0.1 M tetrathiafulvalene (TTF, Sigma-Aldrich, MO, USA) in acetone/ethanol (1:9, v/v) followed by 4 μL of lactate oxidase solution to the anode with intermediate drying steps after each application enabled functionalization of the anode with the mediator and the enzyme. The lactate oxidase

Author Manuscript Author Manuscript Author Manuscript Author Manuscript

solution resulted from dissolving 60 mg/ml lactate oxidase (Toyobo, Japan) in 0.1 M phosphate buffer with 0.25 wt% of glutaraldehyde (Sigma-Aldrich, MO, USA). Drop casting 4 μL of 1 wt% of chitosan (low molecular weight, Sigma-Aldrich, MO, USA) solution over the anode active area completed the anode fabrication process.

Dipping the complete sensor sequentially in solutions of polyvinyl chloride (5 wt% in tetrahydrofuran; Sigma-Aldrich, MO, USA) and edible carbon (5 mg/ml in 0.5 wt% chitosan; Nature's Way, WI, USA) with drying between layers formed the outermost layers of the sensor. Attaching connectors (WM26603-ND, Molex, IL, USA) with conductive silver epoxy (8331D, MG Chemicals, Canada) and passivating the contacts with marine epoxy (Epoxy Marine, Loctite, CT, USA) completed the sensor fabrication. Incubating the sensors in phosphate buffer at 4 °C for 3 days facilitated stabilization of the various polymeric sensor coatings and prepared the sensors for subsequent in vitro and in vivo testing.

Fabrication of wireless electronic module

Laser ablation processing (ProtoLaser U4, LPKF Laser & Electronics, Germany) fabricated flexible printed circuit boards (fPCBs) from commercial double-sided laminated copper (18 μm) – polyimide (75 μm) – copper (18 μm) multi-layer stacks (Pyralux AP8535R, Dupont, DE, USA). Fast drying silver paint (Cat. No. 16040-30, Ted Pella, CA, USA) filled the via holes to connect electrical traces on both sides of the fPCB. Finally, low melt temperature solder paste (SMDLTLFP10T5, ChipQuick, Canada) and air flow soldering connected all electronic components to the fPCB and completed the wireless electronic module fabrication.

Operation of the wireless electronic module

A microcontroller (Attiny84, Atmel Corporation, CA, USA) running firmware controlling two operation modalities (idle, active) provided user control on demand via a graphic user interface implemented in MATLAB (MathWorks, CA, USA). Disabling two n-MOSFET electrically isolated the sensor in the idle state, which prevented sensor discharging. Microcontroller activation of the solid-state switch using a digital output pin during the active modality allowed the sensor voltage to be read across a 100 kΩ resistor connected to the analog to digital converter input pin. Voltage digitization at a sampling rate of 2 Hz and 10 on-chip sample averaging generated a stable measurement signal. Synchronizing a 32-byte cyclic buffer of indexed data in the memory of the NFC chip (M24LR04E, STMicroelectronics, Switzerland), passing the buffer of indexed data to the user application every two seconds, compiling eight indexed data points into a given data reading event (filtered to removed redundant elements), and finally plotting and storing the data on the computer memory completed the data recording and visualization.

Wireless power transfer and system integration

Resonant magnetic induction between paired antenna system enabled wireless power transfer to the sensor. A standard mouse cage with 15 cm x 28 cm footprint defined the experimental arena, and a dual-loop conducting cable wrapped around the periphery of the experimental arena formed the primary antenna. A commercial RF power module operating

Author Manuscript Author Manuscript Author Manuscript Author Manuscript

at 13.56 MHz which supported the NFC ISO 15693 communication protocol (Neurolux, IL, USA) provided wireless power transfer and communication. Interfacing the RF module with a desktop computer equipped with graphic user interface enabled uninterrupted operation and communication with the host computer.

Wound healing model

Approval by the Institutional Animal Care and Use Committee (IACUC) at Northwestern University (protocol IS00018748) preceded all in vivo studies. Animals for in vivo studies involved diabetic (db/db) mice (BKS.Cg-m +/+ Leprdb, #000642; homozygous for Leprdb) and healthy mice (C57/BL6J) procured from Jackson Laboratory, ME, USA. Details of the animal model followed the literature (*16*). Briefly, wound creation began by shaving the fur from the dorsal side of each mouse followed by excising dermis using punch biopsy (diameter: 6 mm). Next, suturing sterilized doughnut-shaped acrylate splints (10-mm inner diameter; 12-mm outer diameter) (3M, MN, USA) around the wound with Vetbond (3M, MN, USA) and 6-0 nylon sutures (Ethicon, OH, USA) prevented the healing process via skin contraction. Laminating the sensor to the center of the wound and then covering it with a transparent sterile occlusive dressing (TegaDerm™, 3M, MN, USA) prepared the animals for the study. Mice without the sensor other than replacement of the protecting dressing comprised the control group. Measuring lactate levels three times a day and acquiring digital images on day 1, 5, 7, and 10 post-injury enabled monitoring of the wound healing process. Three blinded observers utilized ImageJ® for estimating percent wound closure.

Tissue processing and immunofluorescence staining

Excising the regenerated wound tissue on day 10 or 30 post injury with a 10-mm biopsy punch (Acuderm, FL, USA), fixing using 4 % paraformaldehyde, and embedding in paraffin prepared tissue samples for tissue processing and histology. Sectioning and staining the samples with hematoxylin and eosin (H&E) enabled visualization of any potential effect of the sensor on tissue morphology.

In vitro biocompatibility test

A mouse fibroblast cell line (L929, ATCC® CCL-1™, ATCC, VA, USA) in associated media (ATCC® 30-2003™, ATCC, VA, USA) maintained and cultured in T-25 flasks according to the manufacturer's protocols provided the cells for biocompatibility testing. Seeding 10,000 cells in a 24 well plate and placing a UV-sterilized anode/cathode pair in each well prepared the testing setup. Following 96 h, resazurin (Sigma Aldrich, MO, USA) assay and a live/dead staining kit (L3224, Invitrogen, MA, USA) performed according to the manufacturer's protocol with fluorescence measurement and imaging using Cytation5 (Biotek, VT, USA) determined cell viability in the presence of the sensor.

Statistical Analysis—Data is represented as mean ± standard deviation (S.D.). S.D. for data reported in Figure S3, S4, and S5C is calculated based on sensor data points captured during the last 1 min of data recording. Statistical analysis was carried out using Microsoft Excel and Origin Software.

Author Manuscript Author Manuscript Author Manuscript Author Manuscript

Supplementary Material

Refer to Web version on PubMed Central for supplementary material.

Acknowledgment

Research reported in this publication was supported by Defense Advanced Research Projects Agency (D20AC00004) and Center for Advanced Regenerative Engineering (CARE) at Northwestern University. Imaging work was performed at the Northwestern University Center for Advanced Molecular Imaging supported by NCI CCSG P30 CA060553 awarded to the Robert H Lurie Comprehensive Cancer Center. This work made use of the NUFAB facility of Northwestern University's NUANCE Center, which has received support from the SHyNE Resource (NSF ECCS-2025633), the IIN, and Northwestern's MRSEC program (NSF DMR-1720139). A.J.B. acknowledges support from the National Science Foundation Nanoscience Engineering Research Center for Advanced Self-Powered Systems of Integrated Sensors and Technologies (EEC-1160483). J.W.S. acknowledges support from the National Institute of Diabetes and Digestive and Kidney Diseases (grant no. R01DK131302).

References

[1]. Theocharidis G, Yuk H, Roh H, Wang L, Mezghani I, Wu J, Kafanas A, Contreras M, Sumpio B, Li Z, Wang E, Chen L, Guo CF, Jayaswal N, Katopodi X-L, Kalavros N, Nabzdyk CS, Vlachos IS, Veves A, Zhao X, Nat. Biomed. Eng 2022, 6, 1118. [PubMed: 35788686]

[2]. Sen CK, Adv. Wound Care 2021, 10, 281.

[3]. Olsson M, Järbrink K, Divakar U, Bajpai R, Upton Z, Schmidtchen A, Car J, Wound Repair Regen. 2019, 27, 114. [PubMed: 30362646]

[4]. Goldberg SR, Diegelmann RF, Surgical Clinics 2020, 100, 681. [PubMed: 32681869]

[5]. Haalboom M, Blokhuis-Arkes M, Beuk R, Meerwaldt R, Klont R, Schijffelen M, Bowler P, Burnet M, Sigl E, van der Palen J, Clin. Microbiol. Infect 2019, 25, 629.

[6]. Gould L, Li WW, Wound Repair Regen. 2019, 27, 201. [PubMed: 30767334]

[7]. Lu S-H, Samandari M, Li C, Li H, Song D, Zhang Y, Tamayol A, Wang X, Sens. Actuators Rep 2022, 4, 100075.

[8]. Wang C, Shirzaei Sani E, Gao W, Adv. Funct. Mater 2022, 32, 2111022. [PubMed: 36186921]

[9]. Shirzaei Sani E, Xu C, Wang C, Song Y, Min J, Tu J, Solomon SA, Li J, Banks JL, Armstrong DG, Gao W, Sci. Adv 2023, 9, eadf7388. [PubMed: 36961905]

[10]. Yang SM, Kim H, Ko G-J, Choe JC, Lee JH, Rajaram K, An B, Han WB, Kim D-J, Shin J-W, Jang T-M, Kang H, Han S, Lee K, Oh SJ, Hwang S-W, Nano Today 2022, 47, 101685.

[11]. Mostafalu P, Tamayol A, Rahimi R, Ochoa M, Khalilpour A, Kiaee G, Yazdi IK, Bagherifard S, Dokmeci MR, Ziaie B, Sonkusale SR, Khademhosseini A, Small 2018, 14, 1703509.

[12]. Guinovart T, Valdés-Ramírez G, Windmiller JR, Andrade FJ, Wang J, Electroanal. 2014, 26, 1345.

[13]. Bhushan P, Umasankar Y, RoyChoudhury S, Hirt PA, MacQuhaec FE, Borda LJ, Lev-Tov HA, Kirsner RS, Bhansali S, J. Electrochem. Soc 2019, 166, B830.

[14]. Gao Y, Nguyen DT, Yeo T, Lim SB, Tan WX, Madden LE, Jin L, Long JYK, Aloweni FAB, Liew YJA, Tan MLL, Ang SY, Maniya S, Abdelwahab I, Loh KP, Chen C-H, Becker DL, Leavesley D, Ho JS, Lim CT, Sci. Adv 2021, 7, eabg9614. [PubMed: 34020961]

[15]. Xiong Z, Achavananthadith S, Lian S, Madden LE, Ong ZX, Chua W, Kalidasan V, Li Z, Liu Z, Singh P, Yang H, Heussler SP, Kalaiselvi SMP, Breese MBH, Yao H, Gao Y, Sanmugam K, Tee BCK, Chen P-Y, Loke W, Lim CT, Chiang GSH, Tan BY, Li H, Becker DL, Ho JS, Sci. Adv 2021, 7, eabj1617. [PubMed: 34797719]

[16]. Song JW, Ryu H, Bai W, Xie Z, Vázquez-Guardado A, Nandoliya K, Avila R, Lee G, Song Z, Kim J, Lee M-K,Liu Y, Kim M, Wang H, Wu Y, Yoon H-J, Kwak SS, Shin J, Kwon K, Lu W, Chen X, Huang Y, Ameer GA, Rogers JA, Sci. Adv 2023, 9, eade4687. [PubMed: 36812305]

[17]. Jiang Y, Trotsyuk AA, Niu S, Henn D, Chen K, Shih C-C, Larson MR, Mermin-Bunnell AM, Mittal S, Lai J-C, Saberi A, Beard E, Jing S, Zhong D, Steele SR, Sun K, Jain T, Zhao E, Neimeth CR, Viana WG, Tang J, Sivaraj D, Padmanabhan J, Rodrigues M, Perrault DP,

Author Manuscript Author Manuscript Author Manuscript Author Manuscript

Chattopadhyay A, Maan ZN, Leeolou MC, Bonham CA, Kwon SH, Kussie HC, Fischer KS, Gurusankar G, Liang K, Zhang K, Nag R, Snyder MP, Januszyk M, Gurtner GC, Bao Z, Nat. Biotechnol 2023, 41, 652. [PubMed: 36424488]

[18]. Wang L, Zhou M, Xu T, Zhang X, Chem. Eng. J 2022, 433, 134625.

[19]. He X, Yang S, Liu C, Xu T, Zhang X, Adv. Healthcare Mater 2020, 9, 2000941.

[20]. Hunt TK, Aslam RS, Beckert S, Wagner S, Ghani QP, Hussain MZ, Roy S, Sen CK, Antioxid. Redox Signal 2007, 9, 1115. [PubMed: 17567242]

[21]. Britland S, Ross-Smith O, Jamil H, Smith AG, Vowden K, Vowden P, Biotechnol. Prog 2012, 28, 917. [PubMed: 22581665]

[22]. Trabold O, Wagner S, Wicke C, Scheuenstuhl H, Hussain MZ, Rosen N, Seremetiev A, Becker HD, Hunt TK, Wound Repair Regen. 2003, 11, 504. [PubMed: 14617293]

[23]. Porporato PE, Payen VL, De Saedeleer CJ, Préat V, Thissen J-P, Feron O, Sonveaux P, Angiogenesis 2012, 15, 581. [PubMed: 22660894]

[24]. Nareika A, He L, Game BA, Slate EH, Sanders JJ, London SD, Lopes-Virella MF, Huang Y, Am. J. Physiol. Endocrinol. Metab 2005, 289, E534. [PubMed: 15941782]

[25]. Beckert S, Farrahi F, Aslam RS, Scheuenstuhl H, Königsrainer A, Hussain MZ, Hunt TK, Wound Repair Regen. 2006, 14, 321. [PubMed: 16808811]

[26]. Ghani QP, Wagner S, Becker HD, Hunt TK, Hussain MZ, Meth. Enzymol 2004, 381, 565.

[27]. Wagner S, Hussain MZ, Hunt TK, Bacic B, Becker HD, Wound Repair Regen. 2004, 12, 368. [PubMed: 15225216]

[28]. Formby B, Stern R, Biochem. Biophys. Res. Commun 2003, 305, 203. [PubMed: 12732217]

[29]. Baracu AM, Gugoasa LAD, J. Electrochem. Soc 2021, 168, 037503.

[30]. Tehrani F, Teymourian H, Wuerstle B, Kavner J, Patel R, Furmidge A, Aghavali R, Hosseini-Toudeshki H, Brown C, Zhang F, Mahato K, Li Z, Barfidokht A, Yin L, Warren P, Huang N, Patel Z, Mercier PP, Wang J, Nat. Biomed. Eng 2022, 6, 1214. [PubMed: 35534575]

[31]. Vinoth R, Nakagawa T, Mathiyarasu J, Mohan AV, ACS Sens. 2021, 6, 1174. [PubMed: 33517662]

[32]. Yu Y, Nyein HYY, Gao W, Javey A, Adv. Mater 2020, 32, 1902083.

[33]. Ates HC, Nguyen PQ, Gonzalez-Macia L, Morales-Narváez E, Güder F, Collins JJ, Dincer C, Nat. Rev. Mater 2022, 7, 887. [PubMed: 35910814]

[34]. Terse-Thakoor T, Punjiya M, Matharu Z, Lyu B, Ahmad M, Giles GE, Owyeung R, Alaimo F, Shojaei Baghini M, Brunyé TT, Sonkusale S, npj Flex. Electron 2020, 4, 18.

[35]. Brown MS, Browne K, Kirchner N, Koh A, ACS Sens. 2022, 7, 1996. [PubMed: 35797971]

[36]. Ashley BK, Brown MS, Park Y, Kuan S, Koh A, Biosens. Bioelectron 2019, 132, 343. [PubMed: 30897541]

[37]. Brown MS, Ashley B, Koh A, Front. Bioeng. Biotechnol 2018, 6, 47. [PubMed: 29755977]

[38]. Bandodkar AJ, Gutruf P, Choi J, Lee K, Sekine Y, Reeder JT, Jeang WJ, Aranyosi AJ, Lee SP, Model JB, Ghaffari R, Su C-J, Leshock JP, Ray T, Verrillo A, Thomas K, Krishnamurthi V, Han S, Kim J, Krishnan S, Hang T, Rogers JA, Sci. Adv 2019, 5, eaav3294. [PubMed: 30746477]

[39]. Yeknami AF, Wang X, Jeerapan I, Imani S, Nikoofard A, Wang J, Mercier PP, IEEE J. Solid-State Circuits. 2018, 53, 3126.

[40]. Jeerapan I, Sempionatto JR, Pavinatto A, You J, Wang J, J. Mater. Chem. A 2016, 4, 18342.

[41]. Garcia SO, Ulyanova YV, Figueroa-Teran R, Bhatt KH, Singhal S, Atanassov P, ECS J. Solid State Sci. Technol 2016, 5, M3075. [PubMed: 27375962]

[42]. Hickey DP, Reid RC, Milton RD, Minteer SD, Biosens. Bioelectron 2016, 77, 26. [PubMed: 26385734]

[43]. Bollella P, Lee I, Blaauw D, Katz E, ChemPhysChem 2020, 21, 120. [PubMed: 31408568]

[44]. Bollella P, Kadambar VK, Melman A, Katz E, J. Electrochem. Sci. Technol 2022, 2, e2100008.

[45]. Escalona-Villalpando RA, Hasan K, Milton RD, Moreno-Zuria A, Arriaga L, Minteer SD, Ledesma-García J, J. Power Sources 2019, 414, 150.

[46]. Hui Y, Ma X, Cai R, Minteer SD, J. Electrochem. Energy Convers. Storage 2021, 18.

[47]. Chung Y, Ji J, Kwon Y, J. Mater. Chem. C 2019, 7, 11597.

Author Manuscript Author Manuscript Author Manuscript Author Manuscript

[48]. Lee D, Jeong SH, Yun S, Kim S, Sung J, Seo J, Son S, Kim JT, Susanti L, Jeong Y, Park S, Seo K, Kim SJ, Chung TD, Biosens. Bioelectron 2021, 171, 112746. [PubMed: 33113388]

[49]. Carrière M, Buzzetti PHM, Gorgy K, Giroud F, Li H, Borsali R, Cosnier S, Bioelectrochemistry 2023, 150, 108328. [PubMed: 36493673]

[50]. Ryu J, Landers M, Choi S, Biosens. Bioelectron 2022, 205, 114128. [PubMed: 35231752]

[51]. Bandodkar AJ, You J-M, Kim N-H, Gu Y, Kumar R, Mohan AV, Kurniawan J, Imani S, Nakagawa T, Parish B, Parthasarathy M, Mercier PP, Xu S, Wang J, Energy Environ. Sci 2017, 10, 1581.

[52]. Yin L, Moon J-M, Sempionatto JR, Lin M, Cao M, Trifonov A, Zhang F, Lou Z, Jeong J-M, Lee S-J, Xu S, Wang J, Joule 2021, 5, 1888.

[53]. Leiva K, Mahadevan J, Kaile K, Schutzman R, Robledo E, Narayanan S, Muthukrishnan V, Mohan V, Wu W, Godavarty A, Adv. Wound Care 2019, 8, 386.

[54]. Ochoa M, Rahimi R, Zhou J, Jiang H, Yoon CK, Maddipatla D, Narakathu BB, Jain V, Oscai MM, Morken TJ, Oliveira RH, Campana GL, Cummings OW, Zieger MA, Sood R, Atashbar MZ, Ziaie B, Microsyst. Nanoeng 2020, 6, 46. [PubMed: 34567658]

[55]. Castilla DM, Liu Z-J, Velazquez OC, Adv. Wound Care 2012, 1, 225.

[56]. Zhang X, Chen G, Liu Y, Sun L, Sun L, Zhao Y, ACS Nano 2020, 14, 5901. [PubMed: 32315159]

[57]. Chinatangkul N, Pengon S, Krongrawa W, Chansatidkosol S, Limmatvapirat C, Limmatvapirat S, Drug Deliv J. Sci. Technol 2022, 76, 103720.

[58]. Basu A, Heitz K, Strømme M, Welch K, Ferraz N, Carbohydr. Polym 2018, 181, 345. [PubMed: 29253982]

[59]. Egambaram OP, Kesavan Pillai S, Ray SS, Photochem. Photobiol 2020, 96, 779. [PubMed: 31886889]

[60]. Ekstein SF, Hylwa S, Dermatitis 2023.

[61]. Bisht P, Pandey KK, Barshilia HC, Polym. Degrad. Stab 2021, 189, 109600.

[62]. Jarošová R, McClure SE, Gajda M, Jović M, Girault HH, Lesch A, Maiden M, Waters C, Swain GM, Anal. Chem 2019, 91, 8835. [PubMed: 31198034]

[63]. Galliani M, Diacci C, Berto M, Sensi M, Beni V, Berggren M, Borsari M, Simon DT, Biscarini F, Bortolotti CA, Adv. Mater. Interfaces 2020, 7, 2001218.

[64]. Zhu Y, Cankova Z, Iwanaszko M, Lichtor S, Mrksich M, Ameer GA, Proc. Natl. Acad. Sci. U.S.A 2018, 115, 6816. [PubMed: 29891655]

[65]. Muhamed I, Sproul EP, Ligler FS, Brown AC, ACS Appl. Mater. Interfaces 2019, 11, 3771. [PubMed: 30604611]

[66]. Park SA, Teixeira LB, Raghunathan VK, Covert J, Dubielzig RR, Isseroff RR, Schurr M, Abbott NL, McAnulty J, Murphy CJ, Wound Repair Regen. 2014, 22, 368. [PubMed: 24844336]

[67]. Blakytny R, Jude E, Diabet. Med 2006, 23, 594. [PubMed: 16759300]

[68]. Jodheea-Jutton A, Hindocha S, Bhaw-Luximon A, The Foot, 2022, 101909. [PubMed: 36049265]

[69]. Van der Maaten L, Hinton G, Visualizing data using t-SNE. J. Mach. Learn. Res 2008, 9.

[70]. Nussbaumer HJ, Fast Fourier Transform and Convolution Algorithms. Springer, Berlin, Heidelberg 1982.

[71]. Hastie T, Tibshirani R, Friedman JH, Friedman JH, The Elements of Statistical Learning: Data Mining, Inference, and Prediction, Springer, New York 2009.

[72]. Landén NX, Li D, Ståhle M, Cell. Mol. Life Sci 2016, 73, 3861. [PubMed: 27180275]

[73]. Park D-W, Ness JP, Brodnick SK, Esquibel C, Novello J, Atry F, Baek D-H, Kim H, Bong J, Swanson KI, Suminski AJ, Otto KJ, Pashaie R, Williams JC, Ma Z, ACS Nano 2018, 12, 148. [PubMed: 29253337]

[74]. Yang Y, Wu M, Vázquez-Guardado A, Wegener AJ, Grajales-Reyes JG, Deng Y, Wang T, Avila R, Moreno JA, Minkowicz S, Dumrongprechachan V, Lee J, Zhang S, Legaria AA, Ma Y, Mehta S, Franklin D, Hartman L, Bai W, Han M, Zhao H, Lu W, Yu Y, Sheng X, Banks A, Yu X, Donaldson ZR, Gereau RW, Good CH, Xie Z, Huang Y, Kozorovitskiy Y, Rogers JA, Nat. Neurosci 2021, 24, 1035. [PubMed: 33972800]

Author Manuscript Author Manuscript Author Manuscript Author Manuscript

[75]. Zhang Z, Wang W, Jiang Y, Wang Y-X, Wu Y, Lai J-C, Niu S, Xu C, Shih C-C, Wang C, Yan H, Galuska L, Prine N, Wu H-C, Zhong D, Chen G, Matsuhisa N, Zheng Y, Yu Z, Wang Y, Dauskardt R, Gu X, Tok JB-H, Bao Z, Nature 2022, 603, 624. [PubMed: 35322250]

[76]. Rahman MA, Cai L, Tawfik SA, Tucker S, Burton A, Perera G, Spencer MJ, Walia S, Sriram S, Gutruf P, Bhaskaran M, ACS Sens. 2021, 7, 82. [PubMed: 34877860]

Author Manuscript Author Manuscript Author Manuscript Author Manuscript

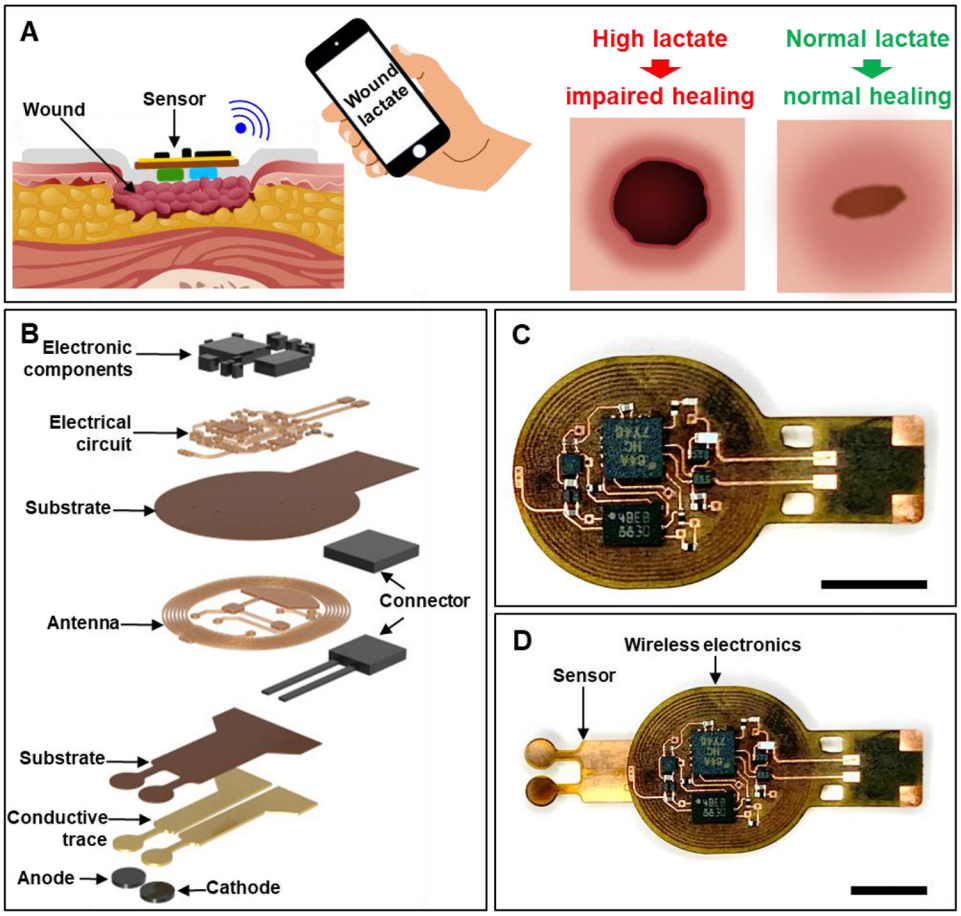

Figure 1.

Wireless, battery-free wound lactate monitor for predicting wound closure. Schematic representation showing (A) the wireless monitoring of wound lactate and its potential use in identifying impaired healing and (B) exploded view of the wireless sensor. Image showing (C) the NFC-based, battery-free wireless electronics and (D) the complete system. (C, D) Scale bar: 5 mm.

Author Manuscript Author Manuscript Author Manuscript Author Manuscript

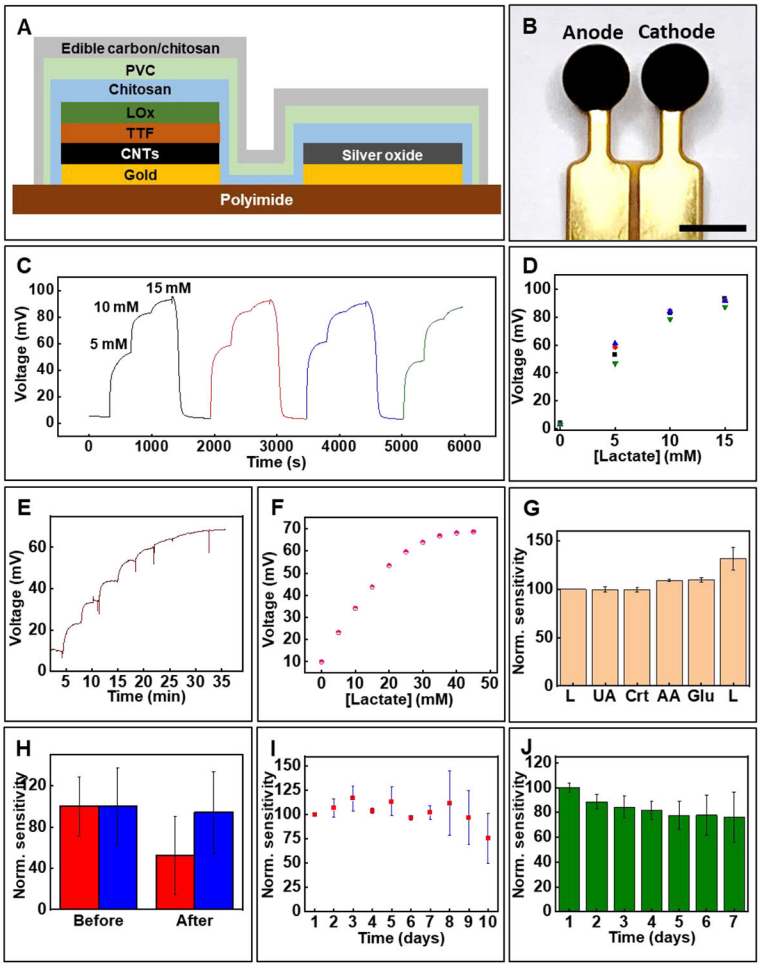

Figure 2.

Key components of biofuel cell-based lactate sensor and its in vitro characterization. (A) Schematic representation showing the key components of the lactate sensor. (B) Image of the lactate sensor. Scale bar 2 mm. (C, D) Reversibility of the lactate sensor signal. (E) Real-time response of the lactate sensor to increasing concentrations and (F) the corresponding calibration plot. (G) Effect of common interfering biochemicals on sensor response. (H) Effect of the UV protective coating on sensor response before and after UV sterilization. Red: without UV protective membrane; Blue: with UV protective membrane (I) Sensor stability studied over a period of 10 days at ambient conditions. (J) Effect of biofouling using artificial wound fluid studied over 7 days. (G-J) Data presented as mean ± S.D., n=3.

Author Manuscript Author Manuscript Author Manuscript Author Manuscript

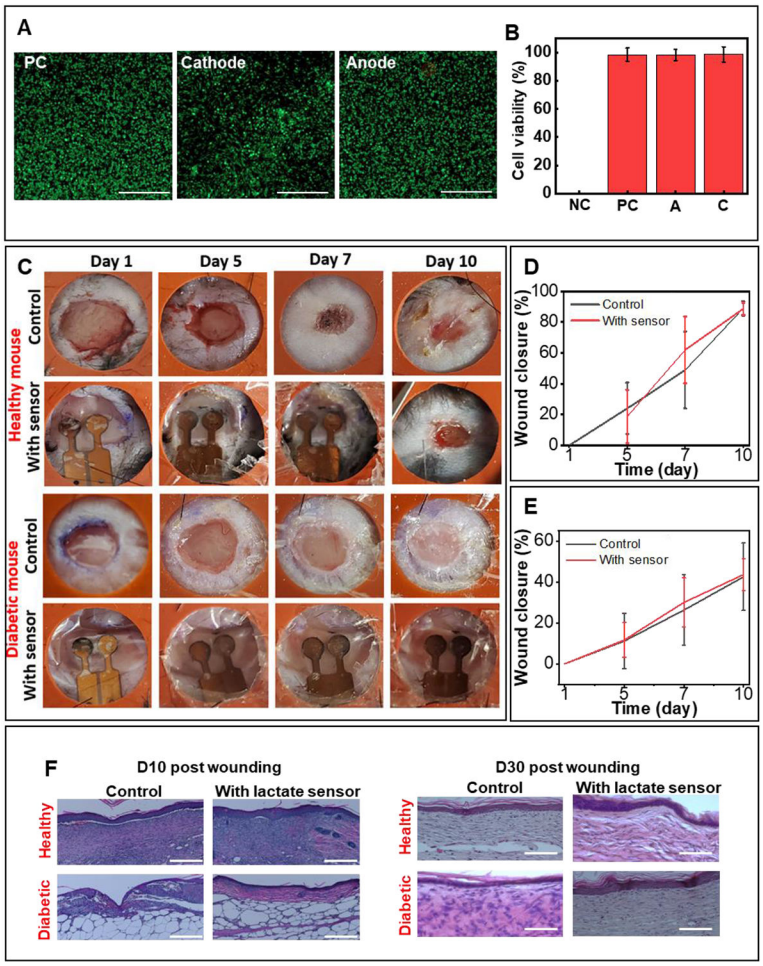

Figure 3.

In vivo biocompatibility of the lactate sensor. (A) Live/dead staining assay of mouse fibroblasts (L929) after 4 days of culture. PC: positive control (no sensor). Scale bar: 500μm. (B) Normalized viability assay data (data presented as mean ± S.D., n=5) (C) Effect of attached sensor on wound closure process. The inner diameter of the splint is 10mm. Quantitative analysis of wound closure with and without sensor for wounds in (D) healthy and (E) diabetic mice. Data presented as mean ± S.D., n=6. (F) Histology of healthy and diabetic mouse with and without the sensor attached after day 10 (partial wound closure) and day 30 (complete wound closure). Scale bar=100 μm.

Author Manuscript Author Manuscript Author Manuscript Author Manuscript

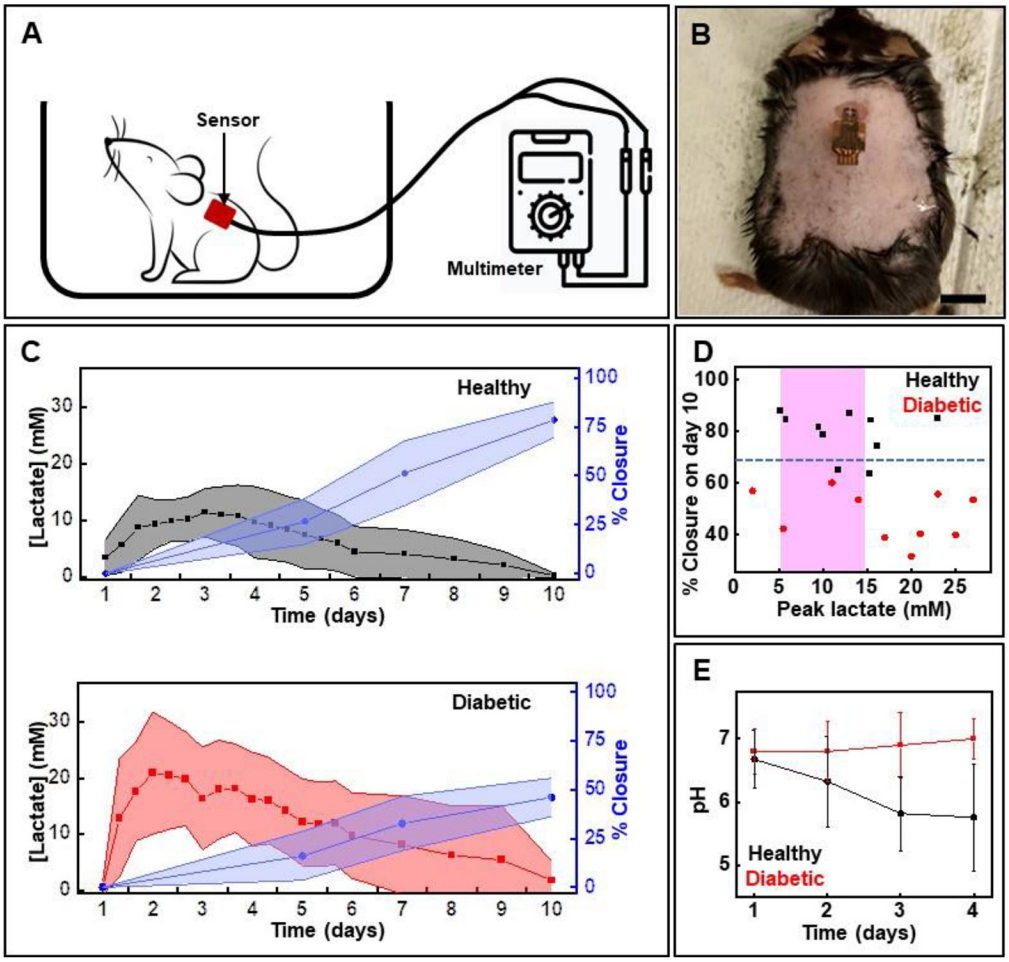

Figure 4.

In vivo studies of the lactate sensor using a mouse model of full thickness dermal wound. (A) Scheme showing the setup for acquiring data using wired sensors (B) Photo of a mouse with the sensor attached onto the wound. Scale bar: 1 cm. (C) Measured lactate levels and % wound closure in healthy and diabetic mice by time (data presented as mean ± S.D., n=10 for each cohort). (D) Relationship between % wound closure on day 10 and lactate level on day 3 of wounding. The pink region shows normal wound lactate range. The blue dotted horizontal line separates wounds that heal normally (wound closure rate > 70% by day 10) from those that show impaired healing (wound closure rate < 70% by day 10). (E) pH levels measured in wounds in healthy and diabetic mice over a period of 4 days (data presented as mean ± S.D, n=6 for each cohort).

Author Manuscript Author Manuscript Author Manuscript Author Manuscript

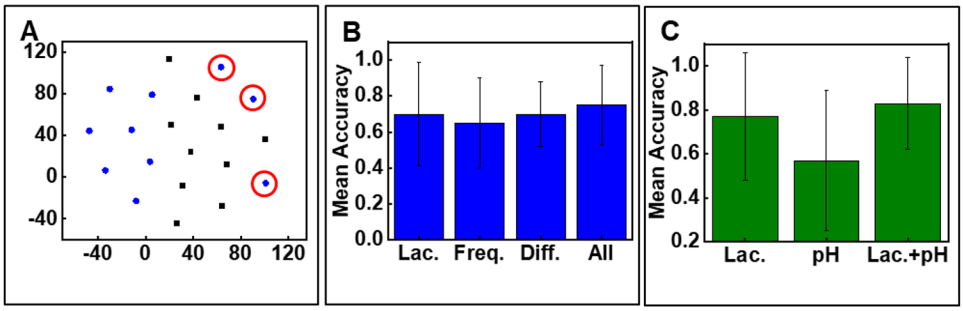

Figure 5.

A mathematical model for predicting wound closure rate. (A) t-SNE visualization of the lactate time series in diabetic group (blue) and healthy group (black). Outliers marked in red circle. (B) Mean classification accuracy of wound closure prediction using each type of feature. Lac.: only lactate time series; Freq: frequency features of the lactate sequence obtained via FFT; All: Lac. + Freq. (C) Combining pH features and lactate features increases the prediction accuracy compared to using only lactate features or pH. (B,C) Data presented as mean ± S.D., n=5.

Author Manuscript Author Manuscript Author Manuscript Author Manuscript

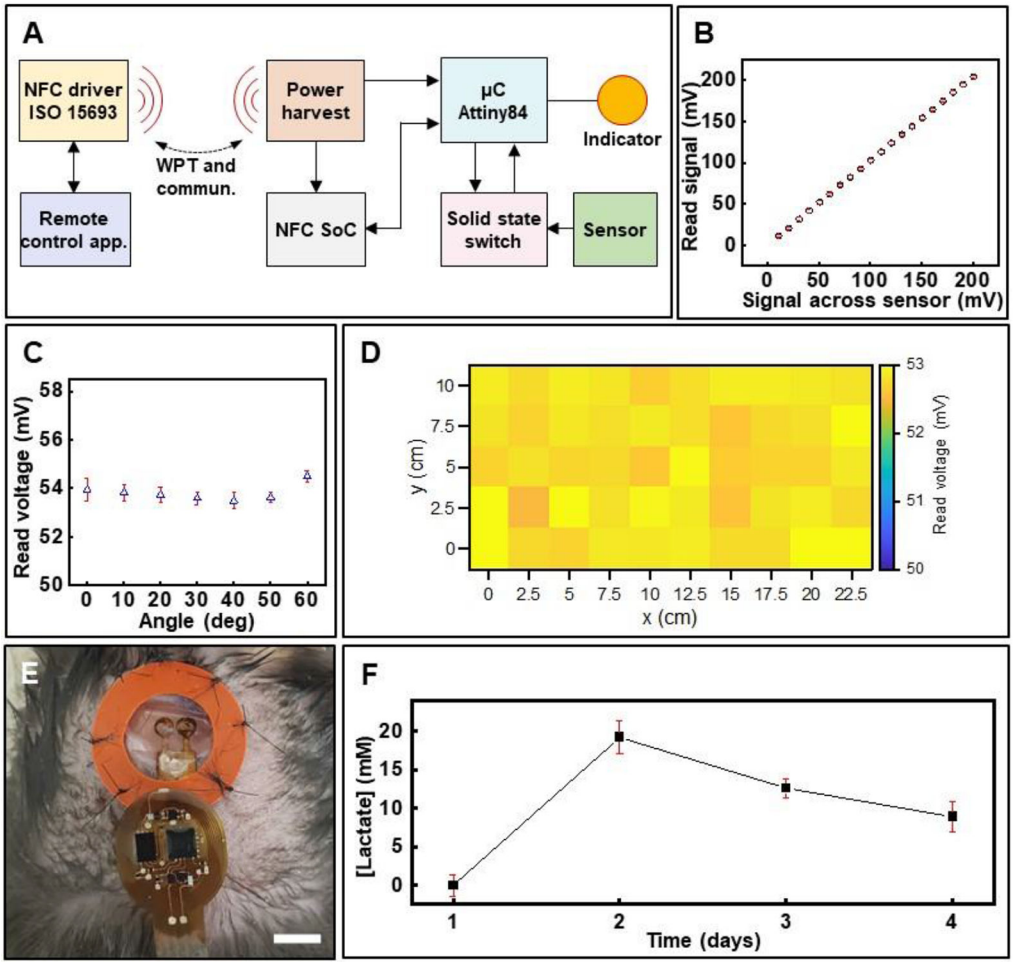

Figure 6.

In vitro and in vivo evaluation of wireless, battery-free wound lactate monitor. (A) Functional block diagram showing the working principle of the wireless electronics for power and data transfer. (B) Correlation between signal output from sensor and that measured by the wireless device (data presented as mean ± S.D., n=3). Effect of performance of the device based on its (C) relative inclination with respect to the transmitter antenna (data presented as mean ± S.D., n=3) and (D) spatial location inside the experimental arena. (E) Photo of the wireless sensor attached to a wound in a diabetic mouse. Scale bar: 5 mm. (F) Daily monitoring of wound lactate in a diabetic mouse over 4 days (data presented as mean ± S.D., n=60).